A Seasonal Climatology of Rossby Wave Breaking in the 320–2000-K Layer

MATTHEW H. HITCHMAN AND AMIHAN S. HUESMANN

Department of Atmospheric and Oceanic Sciences, University of Wisconsin—Madison, Madison, Wisconsin

ABSTRACT

Differential advection in Rossby waves can lead to potential vorticity (PV; P) contours on isentropic surfaces folding over in latitude ($P_y < 0$) in a process called Rossby wave breaking (RWB). Exploring the properties of RWB may shed light on underlying dynamics and enable quantification of irreversible transport. A seasonal climatology of P_y and RWB statistics is presented for the 320–850-K layer using NCEP reanalysis data during 1979–2005 and for the 320–2000-K layer using the Met Office (UKMO) data during 1991–2003. A primary goal is to depict the spatial extent and seasonality of RWB maxima. This analysis shows seven distinct RWB regimes: poleward and equatorward of the subtropical westerly jets, poleward and equatorward of the stratospheric polar night jets, flanking the equator in the stratosphere and mesosphere, equatorward of subtropical monsoon anticyclones, and the summertime polar stratosphere.

A striking PV gradient maximum exists at the equator throughout the layer 360–2000 K, flanked by subtropical RWB maxima, integral components of the Lagrangian cross-equatorial flow. Strong RWB occurs in the polar night vortex where β is small. Over the summer pole, strong poleward RWB associated with synoptic waves decays into small amplitude motions in the upper stratosphere, where heating gradients cause $P_y < 0$. The seven spatial regimes are linked to three different dynamical causes of reversals: wave breaking associated with westerly jets, a combined barotropic/inertial instability in cross-equatorial flow, and on the periphery of monsoon anticyclones.

1. Introduction

L. F. Richardson (1922) anticipated a fundamental aspect of global transport when he linked the bigger whirls' velocity to the lesser whirls' viscosity. Constituents transported globally by large-scale rotational flow can be brought into proximity with constituents originating elsewhere only if there is mixing down to small scales. When finite amplitude (observable) Rossby waves go through their life cycle (Simmons and Hoskins 1978), irreversible mixing occurs, associated with amplification past a breaking point. McIntyre and Palmer (1983, 1984) defined Rossby wave breaking (RWB) to occur when differential advection in eddy motion leads to meridional overturning of potential vorticity (PV; P) contours such that $P_y < 0$. The degree of irreversibility depends on the situation, but in general, the ensuing cascade of enstrophy to smaller scales, modified by secondary instabilities and chaotic advec-

tion in the presence of viscous processes and heat exchange, will lead to significant irreversible transport. Since it is straightforward to calculate $P_y < 0$ and there are a growing number of studies using this or related criteria, we sought to create a more comprehensive RWB climatology, with a view toward future quantification of transport based on RWB.

RWB can occur in association with critical surface absorption of planetary wave activity in the stratosphere, equatorward of the polar night jet. Baldwin and Holton (1988) analyzed P_y reversals on the 850-K surface for boreal winter and showed that RWB is common over the Pacific in the central stratosphere, equatorward of the Aleutian high. Thorncroft et al. (1993) discussed life cycles of midlatitude synoptic waves in a baroclinic zone (jet stream), and categorized events as breaking primarily equatorward (type LC1, anticyclonic), or poleward of the jet (type LC2, cyclonic). Peters and Waugh (1996) explored two different types of poleward wave breaking, where air either wraps up cyclonically (type P1) or anticyclonically (type P2). Hartmann and Zuercher (1998) found a threshold transition from LC1 to LC2 with increasing ambient cyclonic shear in modeled baroclinic life cycles. Esler and

Corresponding author address: M. H. Hitchman, Department of Atmospheric and Oceanic Sciences, University of Wisconsin—Madison, 1225 W. Dayton St., Madison, WI 53706.
E-mail: matt@aos.wisc.edu

Haynes (1999) found that equatorward (poleward) events are initiated by an equatorward (poleward) flux of wave activity, with the difference being linked to jet structure. In this study, we use the term poleward (equatorward) RWB to indicate that the reversal occurs poleward (equatorward) of the seasonal mean jet. Usually both occur at the same time.

Postel and Hitchman (1999) studied RWB at the 350-K surface, which transects the subtropical westerly jets. They found that in the summertime RWB maximizes over the oceans downstream of the monsoon anticyclones. They showed that air in the Southeast Asian monsoon readily mixes with extratropical stratospheric air over the central Pacific in summer, some of which is advected southwestward over the southern Indian Ocean. Similar LC1 surf zone features were noted poleward and downstream of the Mexican high during boreal summer and from Amazonia, Africa, and Indonesia during austral summer. Postel and Hitchman (2001) discussed case studies of the northern Pacific RWB maximum and found that midlatitude synoptic waves traveling north of the Tibetan high break over the mid-Pacific, in association with upward and equatorward refraction toward a critical surface in the tropical tropopause region. Scott and Cammas (2002) studied RWB along the subtropical tropopause and showed that the location of a stagnation point helps determine the strength of a breaking event. They utilized contour stretching as a measure of mixing associated with RWB and emphasized that wave breaking is fundamentally two-way transport, a point also made by Nakamura (2004).

Waugh and Polvani (2000) studied RWB at 350 K in the Pacific during boreal fall–spring, focusing on westerly ducts and intrusion into the Tropics. In a study of RWB in southern winter, Peters and Waugh (2003) showed case studies exploring the relationship between jet structure and sense of wave breaking. Berrisford et al. (2007) studied blocking and RWB in the Southern Hemisphere. To select for blocks they required a reversal strength of −2 PV, with sufficient extent and duration. They found a maximum near 60°S in the South American sector during June–August (JJA), at the downstream end of the Australian subtropical westerly jet.

Other techniques provide information complementary to RWB studies. Orsolini and Grant (2000) studied N_2O laminae in the 500–640-K layer and found enhanced laminae in the surf zones equatorward of the polar night jet, in the Aleutian high, and in the summer stratosphere. A wide variety of methods have been used to estimate stratosphere–troposphere exchange (STE), including the 15-yr climatology by Sprenger and Wernli (2003). Haynes and Shuckburgh (2000a,b) used the coordinate transformation technique of Nakamura (1996) and produced a spatially extensive climatology of effective diffusivity K_{eff} showing minima within the subtropical jets and polar night jets. Shuckburgh et al. (2001) showed that K_{eff} is affected by the QBO in the subtropical stratosphere, which modulates the degree of barotropic instability. Other studies have used regions of nonzero Eliassen–Palm (EP) flux convergence to depict the winter stratospheric and mesospheric surf zones (Sassi et al. 2002). Martius et al. (2007) catalogued the meridional tilt of PV streamers near the tropopause during boreal winter, grouping them into LC1 and LC2 patterns, and explored interannual differences.

Countervailing processes inherent to jets complicate interpretation of RWB. Strong PV gradients associated with westerly jets tend to inhibit RWB, yet the waves exist in meridional temperature gradients that support wave growth and a tendency to break. In an exploration of the degree of inhibition of transport near jet centers, Haynes et al. (2006, manuscript submitted to *J. Fluid Mech.*) employed idealized models to explore the dependence of transport on transience of eddy motion. One goal of our work is to use RWB statistics to better understand the relationship between P_y, RWB frequency, and strength from an observational point of view. A more fundamental goal is to create a comprehensive climatology of RWB statistics for each season from the upper troposphere to the stratopause in order to diagnose spatially coherent, distinct regimes.

Calibration of RWB and transport is beyond the scope of this paper. Here the focus is on describing the distribution of RWB and relating features to underlying dynamical causes. Seven distinct RWB regimes in latitude–altitude are found and three distinctive dynamical causes of RWB are identified.

Some theoretical background is given in section 2. Section 3 describes the data and analysis methods. In section 4, plan views and zonal mean sections of PV gradients and RWB parameters are shown for each season. Synoptic examples of RWB are given. Statistical distributions are explored in order to quantify the relationship between RWB and P_y in different dynamical regimes. In section 5, each spatial regime is discussed, organized by dynamical cause. Section 6 summarizes the main results.

2. Theoretical background

Rossby waves may be regarded most fundamentally as oscillations characterized by significant horizontal displacements, which draw their energy from and

propagate on a PV gradient (Bretherton 1966). At sufficient amplitude, wave motions will overwhelm the zonal mean PV gradient ($\overline{P}_y$), and a Rossby wave breaks:

$$P_y = \overline{P}_y + P'_y < 0, \qquad (1)$$

where Ertel's PV is $P = (\theta_z/\rho)(f + \zeta)$, f is the Coriolis parameter, ζ is relative vorticity, θ is potential temperature, and ρ is the mean density profile (Andrews et al. 1987). The breaking pattern proceeds from the relative inertia of the two fluid masses. The resultant mixing reduces the PV gradient on which the wave was growing, hence waves can limit their growth as $\overline{P}_y \to 0$. The altered mean state is consistent with irreversible tracer transport. Meandering jets can shed eddies, leading to an enstrophy cascade and chaotic advection (Duan and Wiggins 1996; Wiggins and Ottino 2004). Surf zones in jet exit regions encourage subsequent wave breaking, in part reflecting the formation of blocking highs (Nakamura et al. 1997).

With characteristic eddy wind amplitude U and meridional scale L, and neglecting $(\partial\theta_z/\partial y)$, (1) will occur when

$$\frac{U}{L^2} > \beta - \overline{u}_{yy}. \qquad (2)$$

For a given wave amplitude, breaking can be inhibited by a sufficiently strong PV gradient, suggesting that RWB frequency should be inversely correlated with $\overline{P}_y$. For a given PV gradient, a wave can break if it has a sufficiently large eddy wind amplitude or a sufficiently small horizontal scale, suggesting that RWB could occur in large $\overline{P}_y$. The requisite threshold wave amplitude increases in westerly jets, diminishes in easterly jets, and gets smaller approaching the pole where $\beta \to 0$.

Rossby (1947) argued that synoptic wave overturning tends to homogenize absolute vorticity poleward of a westerly jet. McIntyre (1970, 1982) and Rhines and Young (1982) argued that Rossby wave mixing will create sharpened PV gradients at the edges, as illustrated by Butchart and Remsberg (1986). Pierrehumbert (1991) commented that PV gradient enhancements (airmass boundaries) are the direct result of transport. Methven (2003) explored the transport characteristics of the polar vortex edge in a single layer model. An important question with respect to the concept of transport barriers and PV gradients is the degree to which the PV gradients at the edges of a surf zone resulting from a breaking event inhibit subsequent waves from breaking.

In the summer high-latitude stratosphere, static stability decreases poleward, contributing to the possibil-

ity of $\overline{P}_y < 0$ (Shine 1987; Piani and Norton 2002). Birner (2006) found that spatial variations in static stability can have a significant effect on the distribution of P_y.

Consider the zonal mean PV gradient

$$\overline{P}_y = \frac{\overline{\theta}_z}{\rho} \frac{\partial\overline{\eta}}{\partial y} + \frac{\partial}{\partial y}\left(\frac{\overline{\theta}_z}{\rho}\right)\overline{\eta}$$

$$= \frac{\overline{\theta}_z}{\rho}\left[\beta - \overline{u}_{yy} - f\overline{\eta}\left(\frac{\overline{u}_{zz}}{N^2} + \frac{\overline{u}_z}{g}\right)\right] \equiv \frac{\overline{\theta}_z}{\rho}\beta^*, \quad (3)$$

where $\overline{\eta} = f - \overline{u}_y$ is zonal mean absolute vorticity and the thermal wind law, $\overline{\theta}_y = -(f\overline{\theta}_z/N^2)\overline{u}_z$, was used. In square brackets are the beta effect, barotropic term, and baroclinic term. A necessary condition for barotropic instability occurs when $\overline{u}_{yy}$ is large enough to cause $\overline{P}_y < 0$, while a necessary condition for baroclinic instability occurs when $\overline{\eta}\overline{\theta}_{yz}$ causes $\overline{P}_y < 0$ (Fjortoft 1950). This term is modulated by the degree of inertial stability, where $f\overline{\eta} < 0$ indicates inertial instability.

Since RWB creates regions of negative PV gradient, it may facilitate mixing because of barotropic instability (Haynes 1985). Inertial instability in the winter stratosphere and mesosphere (Hitchman et al. 1987; O'Sullivan and Hitchman 1992) and near the subtropical jets (Sato and Dunkerton 2002) facilitates mixing during the RWB process. Inertial instability is relevant at times throughout the tropical troposphere, wherever anomalous PV values ($fP < 0$) are found. Knox and Harvey (2005) describe the geographical distribution of inertial instability and the resulting transport corridors out of the tropical stratosphere.

Wave growth can occur by conversion of zonal mean available potential energy if $-f\overline{\theta}_y\overline{v'\theta'} > 0$ and conversion of zonal mean kinetic energy associated with a jet if $-\overline{u}_y\overline{u'v'} > 0$ (Simmons and Hoskins 1978). The distribution of RWB is linked to sources and sinks in the equation for conservation of Rossby wave activity $A_t + \nabla \cdot \mathbf{F} = S_R$, where $A \equiv \frac{1}{2}\rho\overline{P}_y\overline{\delta y^2}$, $\mathbf{F} = [0, F_{(y)}, F_{(z)}]$ is the EP flux, with components $F_{(y)} = \rho a \cos\phi(\overline{u}_z\overline{v'\theta'}/\overline{\theta}_z - \overline{u'v'})$, $F_{(z)} = \rho a \cos\phi\{[f - (1/\cos\phi)(\overline{u}\cos\phi)_y]\overline{v'\theta'}/\overline{\theta}_z - \overline{u'w'}\}$, $\overline{\delta y^2}$ is a measure of Rossby wave meridional parcel displacement, and S_R represents generation and absorption of Rossby wave activity and attendant irreversible mixing (Andrews et al. 1987). In a seasonal mean, regions of RWB may be associated with a source ($\nabla \cdot \mathbf{F} > 0$) or a sink ($\nabla \cdot \mathbf{F} < 0$).

3. Data and analysis

The National Centers for Environmental Prediction (NCEP) reanalysis fields (Kalnay et al. 1996) during

1979–2005 and UKMO fields (Swinbank and O'Neill 1994) during October 1991–October 2003 were used to calculate PV and RWB statistics from the middle troposphere to near the stratopause. For the NCEP data, daily horizontal winds and temperature at 2.5° resolution and standard pressure levels were used to calculate PV and interpolate to potential temperature levels 320, 330, 340, 350, 360, 370, 380, 400, 420, 450, 500, 550, 600, 650, 750, 850 K on a 5° longitude grid. The UKMO data were treated similarly, with levels extending from 330 to 2000 K.

RWB frequencies were calculated for a variety of threshold reversal strengths in different basic state PV gradients. By imposing auxiliary conditions, one may select for specific regimes. Postel and Hitchman (1999) targeted midlatitude Rossby waves breaking near the subtropical jets by requiring a breaking strength threshold of −1 PV unit (PVU) about the ±1 PVU contours (1 PVU = 10^{-6} m^2 K kg^{-1} s^{-1}). Berrisford et al. (2007) found it useful to screen for blocking highs by requiring a reversal strength of −2 PVU and invoking duration and extent criteria. Here we present results for the simplest, most inclusive criterion, $P_y < 0$. The summer upper stratosphere exhibits $\overline{P}_y < 0$, because of chronic, weak reversals. In this region, the random contour patterns and small amplitudes make the cause of motion hard to identify.

Here, P_y is calculated daily as centered differences across 5° latitude. Since this is comparable to the Rossby radius of deformation, it tends to select for breaking Rossby waves rather than inertia-gravity waves. The number of days of negative P_y per month is converted to a frequency ν expressed as the number of reversal days per 100 days or rpc. The standard deviation of daily values of P_y at each point σ_{P_y} is an indicator of Rossby wave activity. Reversal strength, $S = -P_y$, averaged for reversal days, is useful for distinguishing different RWB regimes. The duration τ, meridional extent L_y, and zonal extent L_x were also calculated for each event. Reversals occur on the flanks of air masses still attached to their parent bodies, as well as on the flanks of separated PV anomalies, hereafter referred to as cutoffs. To the extent that cutoffs are less likely to return to the parent body, the percent of reversals that are cutoffs is an indicator of degree of irreversibility. Nonzero EP flux divergence is used as a separate indication of irreversible generation or absorption.

Results are shown for the December–February (DJF), March–May (MAM), JJA, and September–November (SON) seasons. In Figs. 1 and 2, PV gradient and reversal strength are normalized by the global mean profile of $\overline{P}_y$, to facilitate comparison of RWB

properties across altitude. Since $\overline{\theta}_z/\rho$ increases upward exponentially, dividing by $\overline{\theta}_z/\rho$ tends to deemphasize higher altitudes and higher latitudes. Statistical scatterplots normalized by global mean $\overline{P}_y$ are compared with values normalized by $(\overline{\theta}_z/\rho)\beta \propto \cos\phi$, which tends to emphasize higher latitude features.

4. Seasonal RWB distributions

a. Zonal mean RWB

NCEP seasonal distributions of $\overline{P}_y$ (contours), reversal frequency $\overline{\nu}$ (circle size), and reversal strength $\overline{S}$ (color) are shown for the 320–850-K layer in Fig. 1. Above the tropopause, there is a persistent PV gradient maximum at the equator, flanked by subtropical regions of weak PV gradients that coincide with RWB maxima of moderate frequency. This feature also appears in the UKMO data (Fig. 2). Air flows through this PV gradient maximum from the summer to winter pole in the Brewer–Dobson circulation (Andrews et al. 1987).

The subtropical westerly jets appear as PV gradient maxima, which tilt upward and equatorward along the tropopause, being stronger and more elevated during winter. Chronic RWB occurs both poleward and equatorward of these jets. The regions of weak PV gradient and frequent RWB in the tropical upper troposphere and lower stratosphere (UTLS) are related to the monsoon anticyclones (Postel and Hitchman 1999). This combination of synoptic waves and monsoon anticyclones constitutes the lower transport regime, which readily mixes material into and out of the tropical lower stratosphere (Hitchman et al. 1994). The next subsection shows the horizontal distribution of RWB relative to the jets and monsoons.

A moderate stratospheric polar night jet is seen near 60°N in DJF and a stronger one near 60°S during JJA and SON. Baldwin and Holton (1988) showed that there is an RWB surf zone equatorward of the polar night jet in DJF at 850 K. Here it is seen that this regime extends to all altitudes where the polar night jet is evident. In MAM, the jet is quite weak and is surrounded by a large RWB maximum. There are analogous surf zones equatorward of the SH polar night jet during fall, winter, and spring. As with the subtropical westerly jets, there are two RWB maxima: one poleward and one equatorward of the polar night jet, with poleward wave breaking being stronger and more common. This is qualitatively consistent with Lagrangian calculations by Pierce et al. (1994), who found reduced contour lengthening rates associated with the synoptic-scale flow near the polar night jet axis, with greater values poleward and equatorward of the jet. They suggested
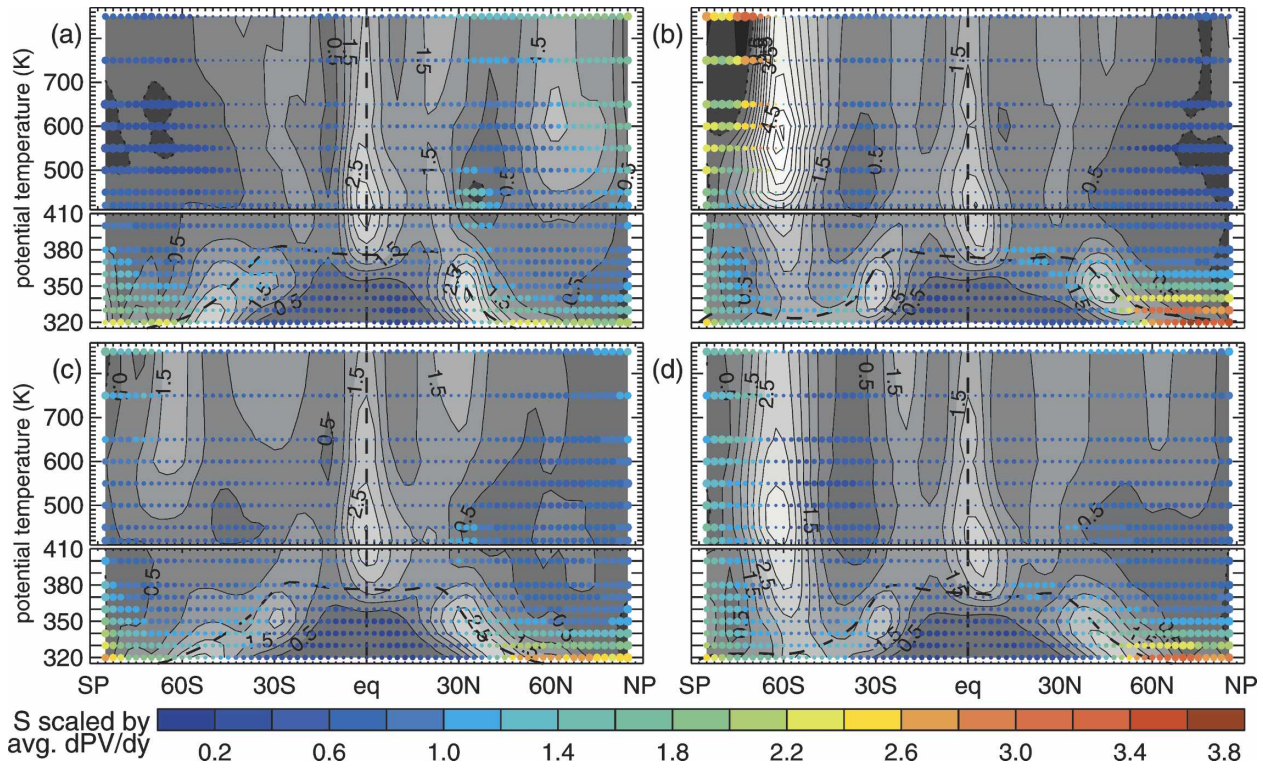
FIG. 1. NCEP seasonal distributions of PV gradient $\overline{P}_y$, normalized by its global, seasonal mean profile (contour interval = 0.5, zero contour dotted), reversal frequency $\overline{v}$ (circle size, maximum 62 reversals per 100 days or rpc), and reversal strength $\overline{S}$, also normalized by the mean $\overline{P}_y$ profile (circle color) for (a) DJF, (b) JJA, (c) MAM, (d) SON.

that mesoscale motions may be important for mixing in and near the jet.

The relationship among frequency, reversal strength, and PV gradient is complex and varies geographically. Large red circles in the summer lower stratosphere and polar night indicate that reversals are strong and common. Large dark blue circles in the summer polar stratosphere indicate weak and common. Small green circles near the subtropical westerly jets indicate medium rare.
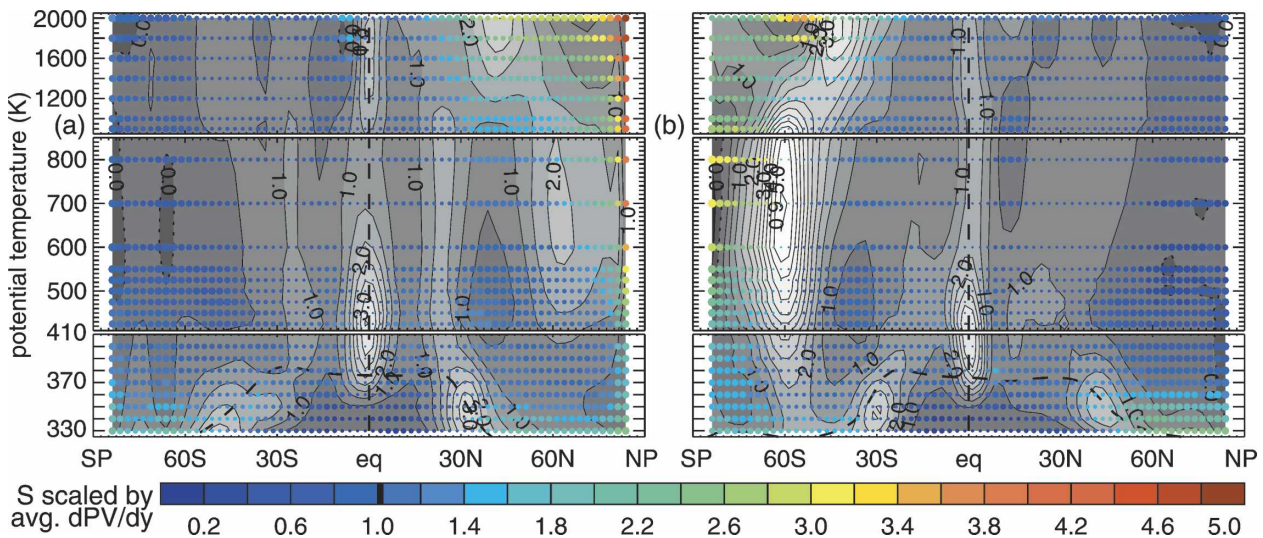
FIG. 2. As in Fig. 1, but for UKMO data for (a) DJF and (b) JJA.

The UKMO seasonal distributions of $\overline{P}_y$, $\overline{\nu}$, and $\overline{S}$ are shown for the 330–2000-K layer and solstice seasons in Fig. 2. Although minor differences may be seen, the UKMO and NCEP data exhibit similar primary features, including the equatorial $\overline{P}_y$ maximum. These latitude–altitude sections exhibit many features that are also similar to distributions of K_{eff} (Haynes and Shuckburgh 2000b, plate 5), including minima in the westerly jets. Differences include significant RWB where K_{eff} is small in the winter and summer polar regimes and the equatorial regime. The summer polar RWB regime extends to 2000 K and is consistent with the region of frequent N_2O laminae in the 500–640-K layer (Orsolini and Grant 2000). The polar night jet tilts abruptly equatorward going into the mesosphere, with a very large region of strong, chronic RWB in the polar vortex. This is the region of the descending separated polar winter stratopause (Hitchman et al. 1989; Garcia and Boville 1994).

b. RWB at 320, 350, 500, and 1600 K

Geographical distributions of P_y, ν, and S for the NCEP data are shown at 320, 350, and 500 K for the solstitial seasons in Fig. 3. The winter hemisphere is characterized by stronger PV gradients than the summer hemisphere, consistent with RWB-driven transport being more active in winter.

The 320-K surface rises from the tropical midtroposphere into the lowest stratosphere over the poles. In the Tropics, significant RWB maxima occur north and south of Indonesia during DJF and over southern Asia during JJA. During DJF, three classic jet streams/storm tracks may be seen in the extratropics, trending eastward and poleward from East Asia, eastern North America, and North Africa. During JJA, the most pronounced feature is a storm track beginning near Australia and extending into the Pacific (Fig. 3b). Reversal maxima may be seen equatorward and poleward of each westerly jet. Poleward breaking typically exhibits stronger reversal strength than equatorward wave breaking.

The 350-K surface lies near 150 hPa, crossing the tropopause near the subtropical jets. In the NH, the subtropical jet exhibits three maxima in all seasons, with greatest intensity during winter (Fig. 3c). These streaks extend from the subtropical central Pacific to the North Atlantic, the subtropical Atlantic to the Middle East, and Southeast Asia to the northeast Pacific. In the SH the subtropical jet stretches from the Indian Ocean across Australia to the eastern South Pacific, lasting from fall until spring, reaching its maximum intensity in JJA (Fig. 3d). Strong RWB is nearly ubiquitous poleward of these jets in both winter and summer. The RWB maximum south of Australia associated with breaking synoptic waves is upstream of the jet exit and chronic region of blocking highs found by Berrisford et al. (2007). Summer polar RWB maxima are evident over the Arctic in JJA (Figs. 3d,f) and Antarctica in DJF (Figs. 3c,e).

In Figs. 3c,d there are frequent, weak reversals equatorward of monsoon anticyclones. During JJA (Fig. 3d) an RWB maximum is seen over the North Pacific and Atlantic, consistent with the results of Postel and Hitchman (1999, 2001). During DJF in the eastern North Pacific (Fig. 3c), equatorward of the subtropical jet, RWB occurs in association with troughs entering the tropical upper troposphere, as shown by Waugh and Polvani (2000).

At 500 K (~21 km, ~50 hPa) a concentrated maximum in PV gradient is seen at the equator, with flanking subtropical minima (Figs. 3e,f). During boreal winter (Fig. 3e), a region of strong P_y, the polar night jet, surrounds the polar vortex in a wave-2 pattern, within which frequent, strong RWB occurs. Equatorward of this jet, an RWB maximum is seen over the North Pacific near the Aleutian high (Harvey and Hitchman 1996), consistent with the results of Baldwin and Holton (1988) for the 850-K surface. During austral winter, RWB is more frequent near Australia (Fig. 3f), but this asymmetry is less pronounced than in northern winter (Fig. 3e). The region of strongest reversals lies within the polar vortex. The distribution of RWB is quite similar to laminae frequency, including the summer high latitude stratosphere (Orsolini and Grant 2000).

The distribution of P_y, ν, and S at 1600 K in the UKMO data is shown for the solstices in Fig. 4. The 1600-K surface lies near 45 km or 1.5 hPa, near the stratopause. The equatorial P_y maximum is quite pronounced, being bracketed by zones of frequent, mild RWB. RWB occurs frequently over the summer poles near the stratopause. At this level, the strongest reversals are found poleward of the polar night jet. The southern polar night jet is nearly zonally symmetric and tilts equatorward with altitude (Fig. 2b). During boreal winter, RWB associated with the Aleutian high creates a long southwestward tongue of high P_y. The Aleutian high is part of a chronic wave one breaking pattern.

Figure 5 shows the distribution of $\overline{\nu}$, cutoff frequency, event duration $\overline{\tau}$, and zonal extent L_x for JJA. Reversal frequency exceeds 50 rpc in the winter polar vortex and approaches 50 rpc in the summer polar stratosphere. Maxima of 20–30 rpc occur in the surf zones equatorward of the polar night jet and near the subtropical jets. Tall maxima of 10–20 rpc occur near 15°N and 15°S in the stratosphere, being larger in the summer hemisphere. Figure 5b shows that cutoff percentage is highly
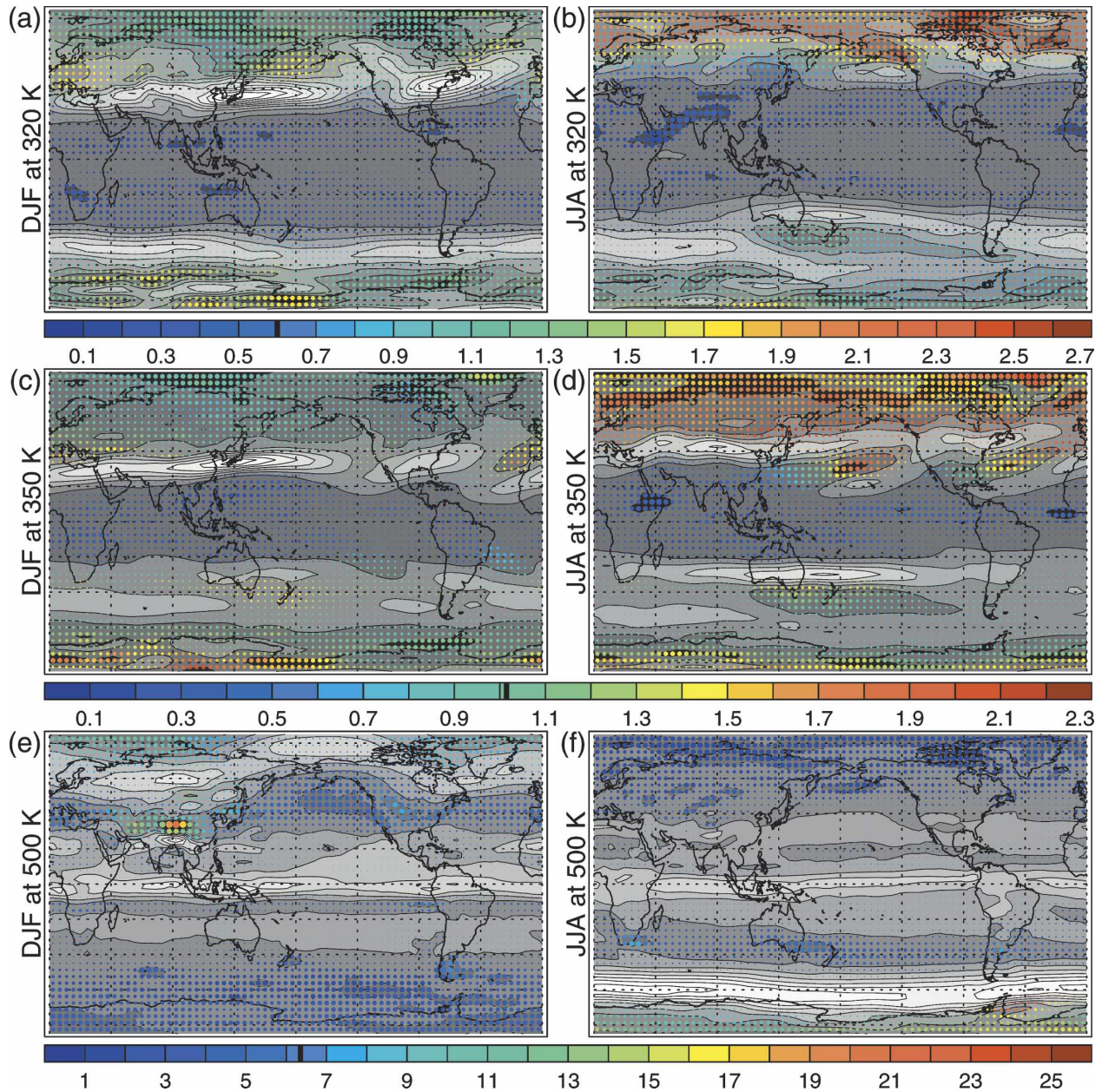
FIG. 3. NCEP seasonal mean $\overline{P}_y$, $\overline{v}$, and $\overline{S}$ at (a),(b) 320, (c),(d) 350, and (e),(f) 500 K, for (a),(c),(e) DJF and (b),(d),(f) JJA. Circle color indicates reversal strength $\overline{S}$, with the thick line on the color bar indicating the global time mean $\overline{P}_y$ at each level. Reversal frequency $\overline{v}$ is indicated by circle size, the largest corresponding to 84 rpc. Contour intervals for $\overline{P}_y$ are 0.4, 1, and 5 PVU $(10°)^{-1}$ at 320, 350, and 500 K. Data for circles were interpolated to a 3.75° latitude grid for clarity.

correlated with $\overline{v}$. RWB events tend to last 2–3 days in most regions of significant v, with zonal extent ~1500–4000 km (Figs. 5c,d). An exception is the summer stratosphere, where reversals last longer and are shorter in zonal scale.

Information regarding possible instability and Rossby wave activity formation, propagation, and absorption is explored in Figs. 6 and 7. Figure 6 shows the

partitioning of $\overline{P}_y$ into $(\overline{\theta}_z/\rho)(\partial\overline{\eta}/\partial y)$ and $\overline{\eta}(\partial/\partial y)(\theta_z/\rho)$ during JJA [cf. Eq. (3)]. White contours show the zonal wind structure, including the polar night jet near 60°S, subtropical westerly jets near 350 K, and the subtropical easterly jet in the summer mesosphere. The winter polar vortex exhibits $P_y < 0$ (Fig. 1b) caused by flow curvature (Fig. 6a). During northern summer, the zero wind line extends upward to 500 K, with weak easterlies
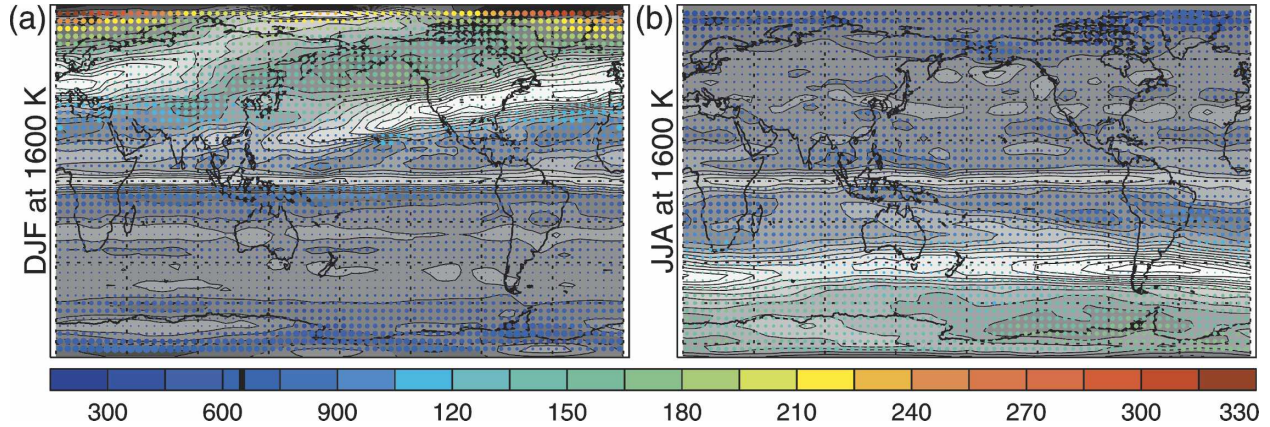
FIG. 4. As in Fig. 3 but for UKMO data at 1600 K, and contour interval = 300 PVU $(10°)^{-1}$. The maximum frequency is 72 rpc.

to the stratopause. This region is characterized by frequent, weak RWB (Fig. 1b). A distinctive negative meridional curvature in zonal wind is noticeable at the equator (Fig. 6a), yielding the equatorial P_y maximum seen in Figs. 1b, 2b. This is present to varying degrees all year.

Enhanced meridional gradients of static stability (Fig. 6b) reduce the region of negative P_y in the polar vortex and lowers the subtropical westerly jets. This factor accounts for $\overline{P}_y < 0$ in the summer polar stratosphere (Fig. 1b).

NCEP EP fluxes and divergences for DJF and JJA are shown in Figs. 7a,b. Synoptic Rossby wave activity excited by baroclinic instability refracts equatorward toward the subtropical tropopause, while planetary wave activity ascends in the winter westerlies, refracting equatorward in the upper stratosphere. The primary pattern of convergence may be viewed as due to upward diminution of poleward heat flux (Figs. 7c,d). In the subtropical and upper stratospheric westerly jets this is significantly modulated by poleward momentum fluxes (equatorward EP fluxes; Figs. 7e,f). The EP flux divergences (convergences) occur just poleward (equatorward) of the subtropical jets, because of barotropic
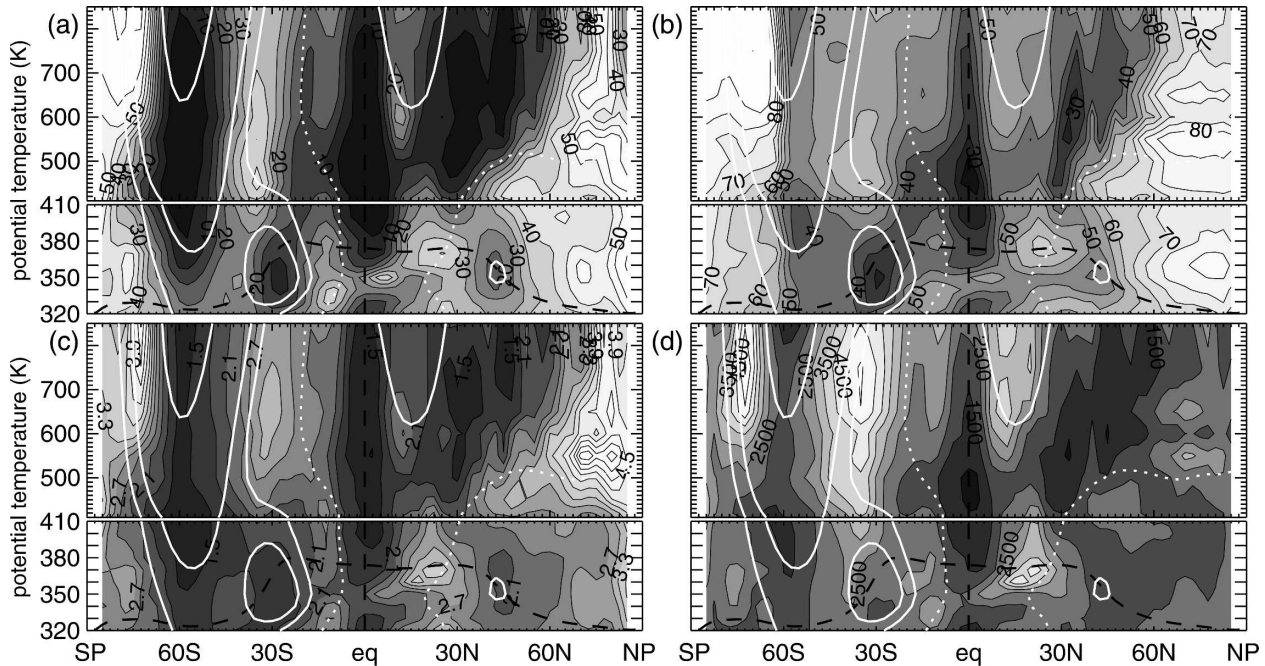
FIG. 5. RWB statistics for JJA in NCEP data (a) $\overline{v}$, contour interval = 5 rpc; (b) cutoff frequency, contour interval = 5 rpc; (c) $\overline{\tau}$, contour interval = 0.3 days; and (d) $\overline{L}_x$, contour interval = 500 km.
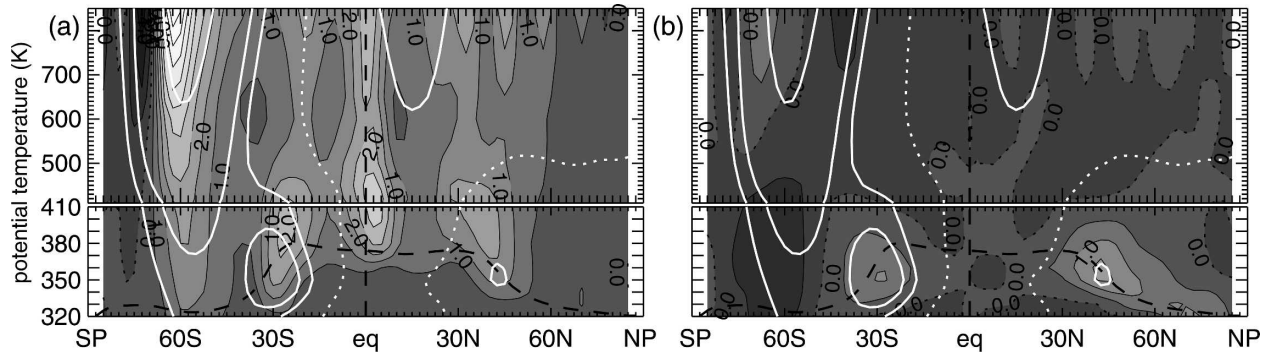
FIG. 6. NCEP JJA distributions of (a) $(\bar{\theta}_z/\rho)[\partial(f - \bar{u}_y)/\partial y]$, contour interval = 0.5; and (b) $(f - \bar{u}_y)(\partial/\partial y)(\bar{\theta}_z/\rho)$, contour interval = 0.5. Solid white contours indicate the -20, 20, 35, and 65 m s^{-1} zonal wind contours. The zero wind line is dotted.

energy conversion during synoptic wave life cycles (Simmons and Hoskins 1978). Near the equatorial tropopause, EP fluxes diverge out of monsoon anticyclones, with significant cross-equatorial momentum transport toward the winter hemisphere. This is related to generation of Rossby wave activity by tropical convection (Postel 1994). Together, monsoons and synoptic waves yield a distinctive pattern of alternating convergence/divergence maxima along the tropopause, which correspond to distinctive RWB regimes (Figs. 1 and 3). In the winter stratosphere, EP fluxes are convergent into the stratospheric surf zones. Weak EP flux divergences are seen in the summer subtropical stratosphere and in the stratospheric polar vortex, raising the possibility of mild in situ generation of Rossby wave activity (Figs. 7a,b).

1) SYNOPTIC EXAMPLES AND DYNAMICAL RWB TYPES

To gain a better appreciation of the structure of RWB in different regions, synoptic examples are shown for selected dates in 2003. Sections at 450 K and 62.5°W on 21 August (Figs. 8a,b) highlight the southern winter stratosphere. A prominent poleward wave breaking event into the polar vortex is seen at 450 K over the Palmer Peninsula, while weaker equatorward breaking events occurred near 40°S, 65°W and 50°S, 120°W. Both the equatorward and poleward breaking regimes are deep (Fig. 8b) and are related to the same traveling planetary wave. These figures show that poleward and equatorward wave breaking can occur from the same planetary wave propagating on the polar night jet. A similar relationship may be seen for the synoptic Rossby wave breaking on the subtropical westerly jet on 8 July (Figs. 8c,d), where equatorward and poleward wave breaking occur near 25° and 50°N.

It may be useful to view this classical poleward and

equatorward wave breaking on subtropical and polar night jets from a unified perspective where there is a common underlying dynamical origin. We suggest categorization of this type of breaking as westerly jet RWB, with equatorward and poleward subtypes as defined by Thorncroft et al. (1993), and further subtypes of poleward wave breaking by Peters and Waugh (1996). At high latitudes during northern summer, a distinctive poleward RWB regime is seen near 75°N in Figs. 8c,d. These synoptic waves travel slowly relative to the mean flow, due to small β, and extend into the summer stratosphere in weak flow, with critical surfaces well into the stratosphere (cf. Fig. 6a).

On July 23, a classic equatorward wave breaking event occurred on the westerly jet near 50°–70°N, in the 330–400-K layer (Figs. 8e,f). Near 70°N, milder, poleward wave breaking occurs, extending upward to ~450 K. In Fig. 8e, an RWB maximum extends southwestward across China from the primary breaking event near 157.5°E, indicating the presence of a PV streamer. Near 20°N, 157.5°E another RWB maximum extends southwestward on the equatorward side of the anticyclone near 40°N, 180°, extending from 320 to 425 K (Fig. 8f). Another occurs near 20°N, 100°E. These PV streamers occur on the equatorward side of subtropical anticyclones. Subtropical anticyclones are reservoirs of small PV that advect extratropical PV streamers around their equatorward sides. This dynamically distinctive cause of reversal suggests categorization as monsoon RWB.

On 12 January at 750 K, RWB occurred over the east coast of Asia, over the North Pacific, and near 10°N and 10°S (Fig. 8g). The PV field indicates the presence of a traveling planetary wave 2 in the northern high latitudes and waves in the Tropics. A meridional section at 162.5°W (Fig. 8h) shows the vertical extent of each RWB patch. The RWB region near 50°N is quite deep,
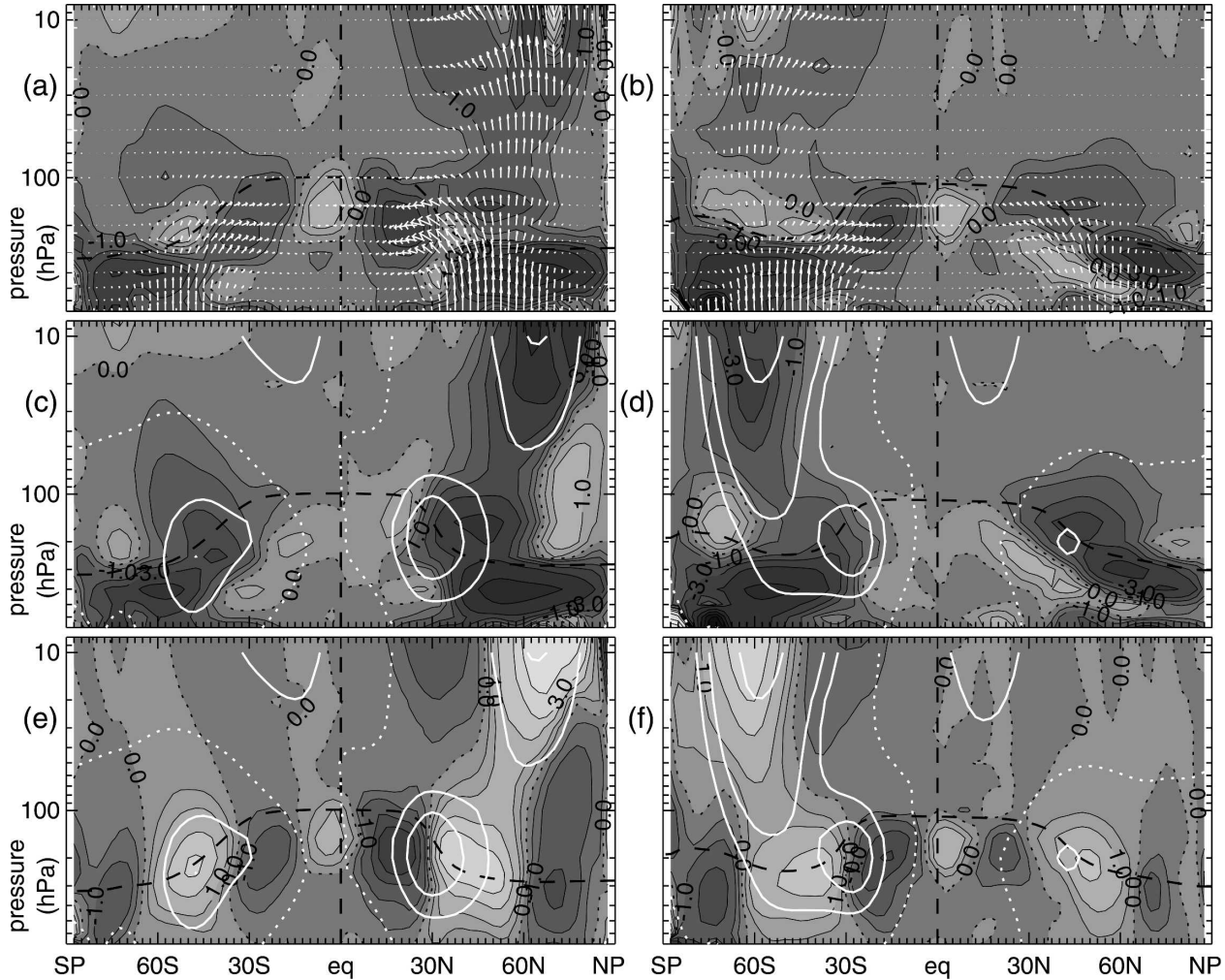
FIG. 7. Eliassen–Palm fluxes and divergences during (a),(c),(e) DJF and (b),(d),(f) JJA; EP fluxes were divided by density prior to plotting. Contour interval = 3 m s^{-1} day^{-1}, except for 0.5 m s^{-1} day^{-1} for values less than 3. (a),(b) Total EP fluxes and divergences, (c),(d) divergences associated with $F_{(z)}$, and (e),(f) divergences associated with $F_{(y)}$. White contours are zonal wind, as in Fig. 6.

consistent with expectations for a breaking planetary wave. The RWB region near 10°S also exhibits deep vertical continuity. In Figs. 1 and 2, note the strongly curved PV field in this region. This dynamically distinctive tropical regime occurs where the flow is inertially and barotropically unstable, suggesting categorization as inertial/barotropic instability RWB.

2) RWB STATISTICS

Statistical relationships among $\overline{P}_y$, $\overline{\nu}$, $\overline{S}$, $\overline{\sigma}_{P_y}$, $\overline{L}_x$, $\overline{\tau}$, and cutoff percent were explored in order to determine how these statistics relate to the PV field and whether there are unique dynamical relationships for distinct RWB regimes. Selected results are described here.

The correlation coefficient between $\overline{S}$ and $\overline{\sigma}_{P_y}$ exceeds 0.9 for both DJF and JJA. Both of these quantities increase with increasing Rossby wave activity. The

correlations between $\overline{S}$ and $\overline{P}_y$ and between $\overline{S}$ and $\overline{\nu}$ are low (not shown), indicating that frequent RWB can be strong or weak, and infrequent RWB can be either strong or weak (cf. Figs. 1 and 2).

Figure 9 shows $\overline{P}_y$ versus $\overline{\sigma}_{P_y}$, both normalized by $(\overline{\theta}_z/\rho)\beta$, for DJF and JJA, with $\overline{\nu}$ increasing from blue to red. In both seasons, reversals increase as the PV gradient decreases and as PV variability increases, in agreement with Eq. (2). The blue region shows that Rossby waves occasionally break in strong PV gradients. A large number of reversals occurs where $\overline{\sigma}_{P_y}$ is large and $\overline{P}_y$ is negative. This is more pronounced during JJA, representing the active northern stratosphere. The region of low reversals, small $\overline{\sigma}_{P_y}$, and large $\overline{P}_y$ is also more pronounced during JJA, representing the stable southern winter vortex. Very few points exist in the upper-right-hand-side corners of Fig. 9, above
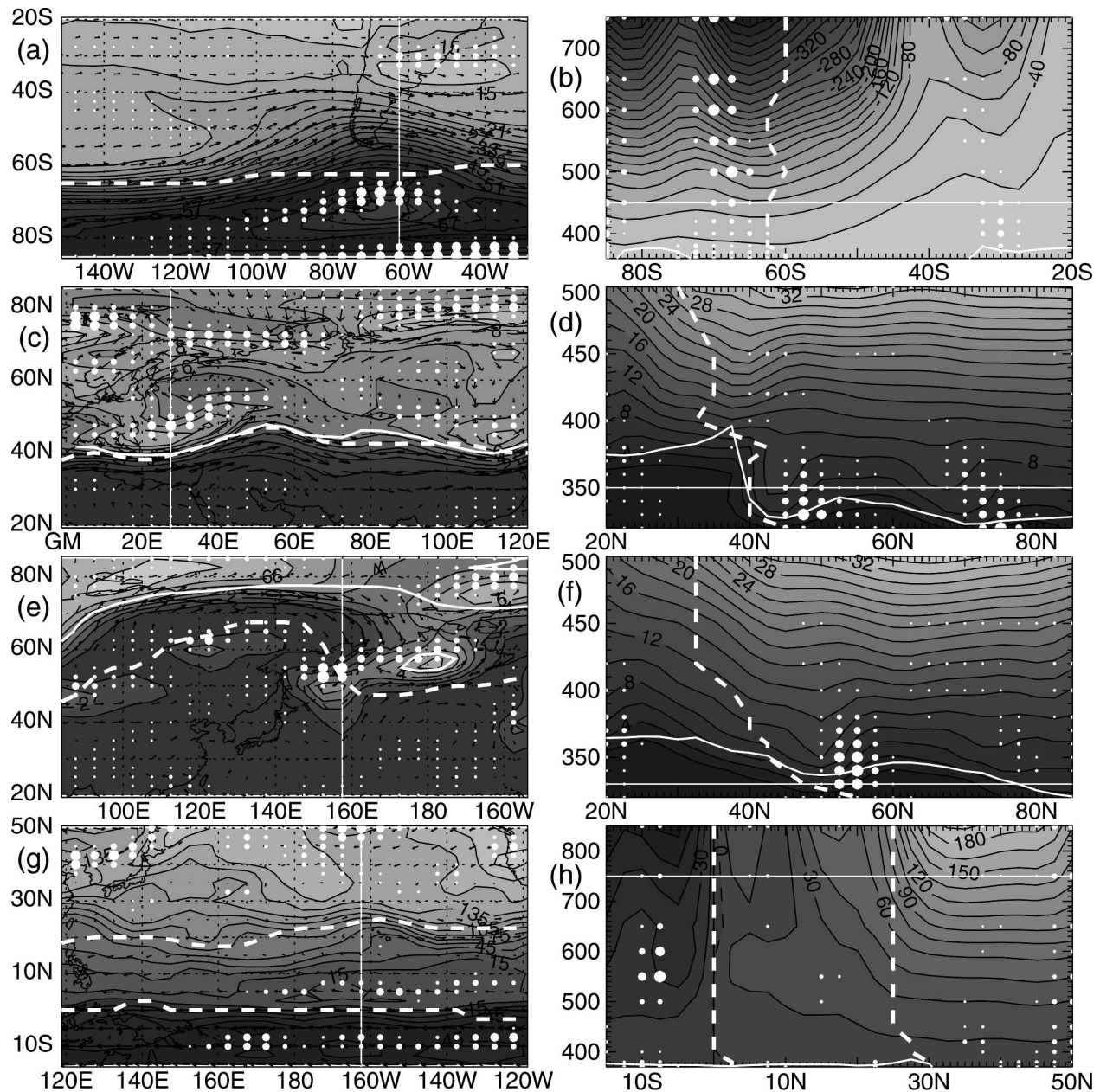
FIG. 8. Plan views and meridional sections of RWB events during 2003 in the NCEP data: (a) 21 Aug, 450 K, contour interval = 3 PVU, (b) 21 Aug, 62.5°W, interval = 20 PVU, (c) 8 Jul, 350 K, interval = 1 PVU, (d) 8 Jul, 27.5°E, interval = 3 PVU, (e) 23 Jul, 330 K, interval = 1 PVU, (f) 23 Jul, 157.5°E, interval = 2 PVU, (g) 12 Jan, 750 K, interval = 15 PVU, and (h) 12 Jan, 162.5°W, interval = 15 PVU. Reversal strength is indicated by circle size. The tropopause is indicated in white, while the thick dashed white lines indicate seasonal mean P_y maxima (jets).

threshold values of variance and PV gradient. Strong wave breaking can limit the PV gradient, while a strong PV gradient can limit breaking.

Based on inspection of Figs. 1 and 2, geographical masks were defined for seven distinct latitude–altitude regions: tropical upper troposphere, equatorward of the subtropical westerly jets, poleward of the subtropical westerly jets, the equatorial stratosphere, equatorward of the winter stratospheric jet, poleward of the winter stratospheric jet, and the summer stratosphere. Figure 10 shows $\bar{v}$ versus $\bar{P}_y$ for DJF and JJA, normalized by the global mean profile of $\bar{P}_y$ and by $(\bar{\theta}_z/\rho)\beta$, with color indicating geographical regime. Summer and winter are shown separately for the region poleward of the tropo-
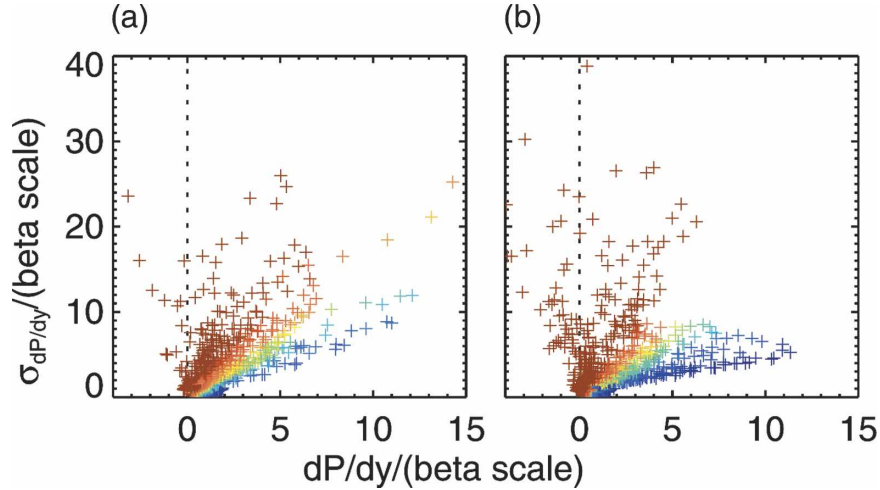
FIG. 9. Scatterplot of $\overline{\sigma}_{P_y}$ vs $\overline{P}_y$, normalized by beta, in NCEP data for (a) DJF and (b) JJA, with highest $\overline{\nu}$ in red, lowest in blue.

pause jet. Normalizing by mean $\overline{P}_y$ (upper) diminishes polar features somewhat, while normalizing by β (lower) amplifies high latitude features. The range is more than twice as large in the lower panels, reflecting the $\sec\phi$ amplification of higher latitudes. Tropical features are drawn into a more compact curve with β scaling.

There is considerable scatter in the $\overline{P}_y$ normalization (upper), with correlation coefficients of -0.65 for DJF and -0.69 for JJA. This suggests that about half of the variance in reversal frequency is related to strength of PV gradient. Higher correlations are obtained within each geographical location, as reflected in the more compact clouds for each color. The tropical upper troposphere (black) exhibits a wide range of reversal frequencies corresponding to small PV gradient. This occurs in an environment where convection homogenizes PV. The equatorial stratosphere (green) shows a similar hockey stick shape, but at much higher PV gradients. The clouds of points to the right correspond to waves breaking near westerly jets. In the upper left, a reversal frequency exceeding 50 rpc implies a time mean negative PV gradient. Again, two groups may be discerned: the summer upper stratosphere (dark red), with small negative PV gradient, and poleward of westerly jets in both the summer and winter (purple, light, and dark blue), where β is small (cf. Figs. 1 and 2). The two seasons are slightly different, with a branch of low-frequency wave breaking at high PV gradient and a branch of high frequency with reversed PV gradient appearing in the southern winter stratosphere (right).

Scaling by β (lower) collapses events in the equatorial stratosphere (green), tropical upper troposphere (black), and summer stratosphere (dark brown) onto a compact curve, which may be fitted with the line $\overline{\nu} \approx$

$50\{1 - [\overline{P}_y/(\overline{\theta}_z/\rho)\beta]\}$. The clouds at medium frequency and larger $\overline{P}_y$ are associated with Rossby waves breaking near the subtropical and polar night jets, where $\overline{P}_y$ is enhanced by curvature of the westerly flow.

Salient features of the statistical relationships suggest the following. Large PV gradients are consistent with infrequent RWB, but waves with a large enough amplitude can overcome a given PV gradient [cf. Eq. (2)]. Breaking strength is linearly related to daily variability but not to PV gradient. The tropical regimes and high latitude summer regime lie on a fairly compact curve in $\overline{\nu} - \overline{P}_y$ space, while waves breaking on jets are typified by a more variable relationship between $\overline{\nu}$ and $\overline{P}_y$. This brief inspection of phase space in Figs. 9 and 10 reveals three distinct dynamical regimes: Reversals occur over a large range in P_y (westerly jet RWB), in a compact curve for the tropical UTLS (monsoon RWB), and in a compact curve for the tropical middle atmosphere (inertial/barotropic RWB). The upper polar summer stratosphere exhibits a similar compact curve in a region where $\overline{P}_y < 0$. It will be treated as a special case of westerly jet RWB.

5. Discussion

Discussion of the seven spatial RWB regimes is grouped under three distinct RWB processes. The most familiar type, westerly jet RWB, will be discussed first, focusing on interpretation of subtropical westerly jets, the subtropical edge of the stratospheric surf zone, and RWB in the polar night. The nature of RWB in the summer stratosphere is explored as an upward extension of poleward breaking near the tropopause jet. Next, RWB in the tropical UTLS, monsoon RWB, will be
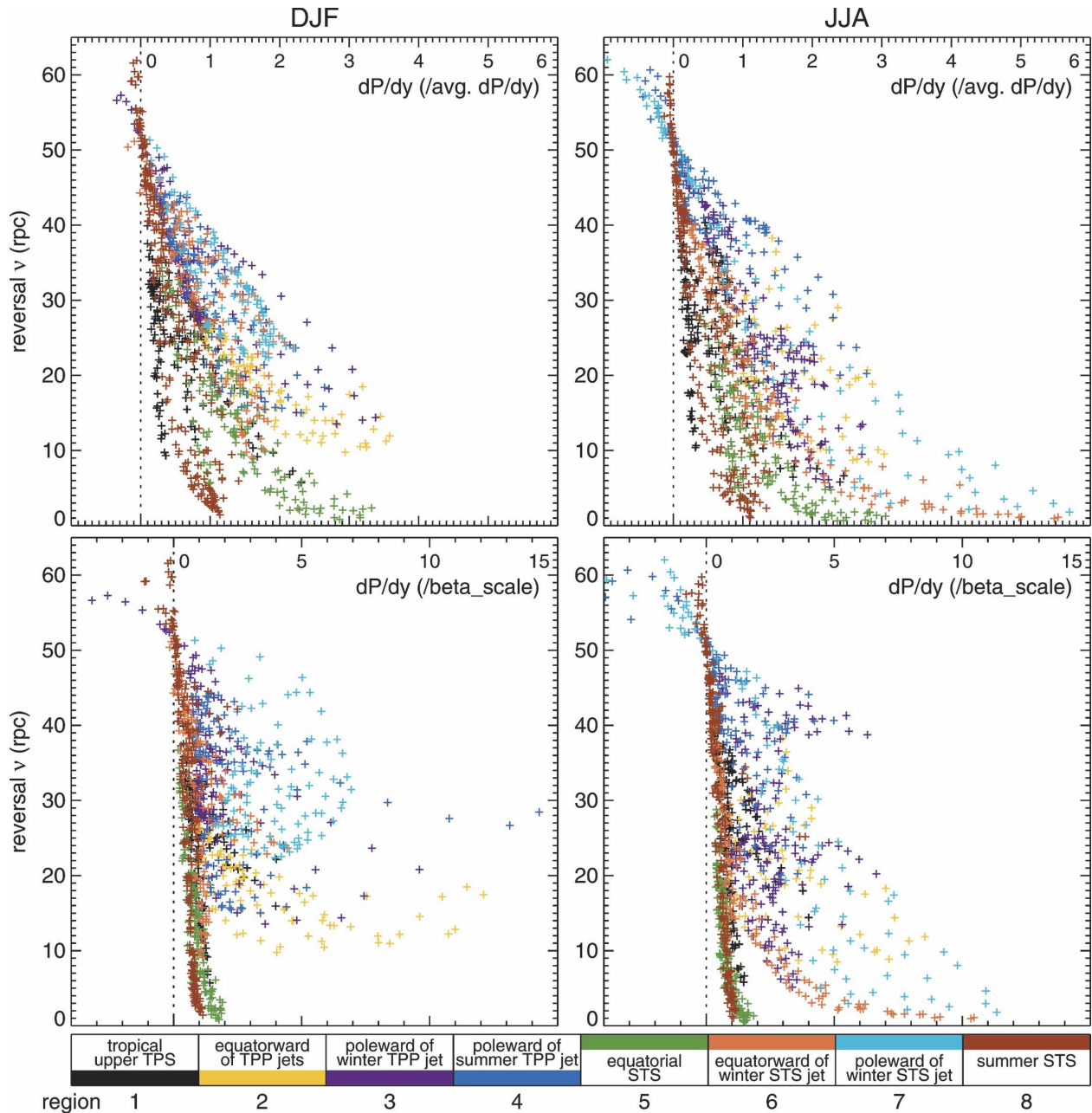
FIG. 10. Scatterplots of $\overline{P}_y$ vs $\overline{v}$ (rpc) for DJF and JJA. (top) Normalization is by the global mean profiles of $\overline{P}_y$, and (bottom) by $(\overline{\theta}_z/\rho)\beta$. Points are colored by geographical region.

discussed. Finally, RWB flanking the equatorial P_y maximum, inertial/barotropic RWB, will be investigated.

a. Westerly jet RWB

Baroclinic instability leads to synoptic Rossby waves going through their life cycles in the vicinity of critical surfaces on the flanks of upper-tropospheric westerly jets. Planetary scale waves break in the vicinity of critical surfaces on the flanks of the polar night jet. Both

scales of Rossby waves exhibit poleward and equatorward wave breaking, suggesting that there is an underlying similarity in the critical surfaces flanking westerly jets. There is a broad scatter in the relationship between v and P_y, distinct from the compact curves for tropical and summer stratospheric RWB.

Although RWB is most fundamentally a two-way exchange (Scott and Cammas 2002; Nakamura 2004), net heating patterns lead to divergence and convergence.

From mass continuity considerations, a poleward and downward meridional circulation in the UTLS is consistent with a bias in favor of poleward breaking near the subtropical jets. Air entering the polar night will cool and sink, suggesting that poleward wave breaking might dominate in the upper polar night vortex. In the lower part, sinking and divergence would be compatible with a shift toward outward or equatorward wave breaking. This general transition is seen in both winters (Figs. 1a,b and 2a,b). By the same principle, wave breaking on the equatorward side of monsoon anticyclones is associated with mass divergence (section 5b).

1) Subtropical westerly jets

The distribution of RWB near the subtropical westerly jets is quite similar to the K_{eff} diagnostic of Haynes and Shuckburgh (2000b). Both diagnostics indicate minima in stirring in the subtropical jets. This is consistent with the idea that locally enhanced P_y at the jet center might tend to inhibit RWB. Stirring within the RWB zones flanking the jet is rapid, with reduced stirring at the jet (Haynes et al. 2006, manuscript submitted to *J. Fluid Mech.*). Rossby wave statistics show that waves of sufficient amplitude sometimes break in the jet centers. Occasional eddy shedding and mesoscale processes contribute to transport across the jet.

Constituent layering is quite strong in the subtropical westerly jets (Danielsen et al. 1991; Kritz et al. 1991; Wilson et al. 1991; Newell et al. 1999; Ray et al. 2005), indicative of active mixing of stratospheric and tropospheric air at mesoscale. Jets are also preferred regions for STE associated with resolved mesoscale motions (Hitchman et al. 2004; Büker et al. 2005). Momentum fluxes also maximize in these jets, in both zonal mean climatologies (Peixoto and Oort 1992) and in the storm tracks (Lau 1978). Hoskins et al. (1985) discuss examples of partly irreversible migrations of PV anomalies across the transiently evolving jet. Figure 7 shows that each subtropical jet coexists with an EP flux convergence/divergence dipole, implying changes in the mean state, hence irreversible transport. An analogous situation exists in oceanic western boundary currents, where the PV gradient maximum exists at the current maximum (Bower 1991). The presence of warm and cold core eddies is proof of water mass exchange across the time mean jet (Doglioli et al. 2006). Although there is a minimum in large-scale stirring in these jets, some transport occurs via coherent fluid masses crossing the time mean jet and by mesoscale mixing.

The manner in which PV contours bend across a time mean jet axis may contribute toward a minimum in reversal frequency at the jet. Consider the example in Fig. 8e, where air is transported both ways across the time mean jet axis (dashed white line). A tropical low PV air mass surges northeastward, while a high PV air mass surges southwestward, creating PV reversals in between. At the eastern edge of the poleward-surging air mass, PV contours are aligned along meridians so there is no reversal signature, despite the fact that some of this air remained well north of its original position, beyond the time mean jet. Thus, significant material transport can occur across the time mean jet axis even though PV reversals are weaker and less common than on the jet flanks. This process is visible in many synoptic sequences that we have examined, where the evolving jet breaks and reforms. This aspect can yield RWB maxima straddling the jet even though there is transport through the time mean jet. In the shear zones flanking a jet, contour deformation will readily fold over PV contours on both sides. When air masses cross the time-mean jet axis, PV contours tend to be oriented perpendicular to the jet axis, so $P_y < 0$ is less common.

The original RWB concept was first applied to the northern winter midlatitude stratospheric surf zone (McIntyre and Palmer 1983; Baldwin and Holton 1988). Tropical air surges poleward around the polar vortex and into the Aleutian high, while polar air wraps equatorward around the Aleutian high (Harvey et al. 1999). Equatorward planetary wave breaking may be viewed as the result of critical surface absorption on the equatorward flank of the polar night jet, similar to synoptic waves over the summer North Pacific (Postel and Hitchman 2001). This equatorward RWB is consistent with mass divergence out of the base of the cold, subsiding polar vortex air. The broad, shallow surf zone associated with quasi-stationary planetary waves 1 and 2 in the NH may be contrasted with the narrow, deep southern winter midlatitude surf zone associated with traveling wave 2 (Figs. 1a,b, and 2). The zonal asymmetry of the northern winter surf zone is quite pronounced (Fig. 3e), but the SH surf zone also exhibits some zonal asymmetry, with more RWB in the Australian sector (Fig. 3f). The existence of these surf zones implies significant Lagrangian transport, which is poleward and downward (Wallace 1978; Kida 1977).

Neu et al. (2003) studied probability distribution functions of long-lived tracers to describe the subtropical edge of this surf zone. From a meteorological point of view, it may be useful to consider the by-product of RWB, where air masses advance poleward and equatorward, with fronts at the leading edges. Tropospheric fronts are characterized by jumps in dynamical and constituent properties across them on short spatial scales and are active mixing zones. This type of structure is also common in the stratospheric subtropics (e.g., Murphy et al. 1993) and near the polar night jet maximum

(e.g., Tuck et al. 1992). They are characterized by jumps in PV and constituents across spatial scales of less than ~100 km. Near the polar night jet there are often several thin PV laminae, a result of differential advection in nearly irrotational flow just equatorward of the jet maximum. Palmen and Newton (1969) defined distinct stratospheric air masses bounded by fronts. These jumps are active mixing zones, as evidenced by enhanced constituent variability in the jumps. The term subtropical stratospheric front may be useful in referring to the jump at the subtropical edge of the stratospheric surf zone, while a subpolar stratospheric front would indicate the jump at the poleward edge in the polar vortex. Just as in the troposphere, subtropical stratospheric fronts are created by differential advection by the large-scale flow, which is balanced by mesoscale mixing processes. The location of these stratospheric fronts is determined by the distribution of planetary wave sources, how the wave activity propagates, and where it is absorbed. This, in turn, is regulated by the location of a critical surface, which is distinct from the frontal locations.

2) POLAR NIGHT SURF ZONES

Poleward RWB is very common within the stratospheric winter polar vortex, especially over Antarctica (Figs. 1b, 2b). It coincides with a region of $\overline{P}_y < 0$, suggesting that energy conversion processes may contribute to Rossby wave activity over the poles. Figure 6 suggest that this is due to $\beta \rightarrow 0$ and large $\overline{u}_{yy}$.

Mixing and waves within the stratospheric polar vortex has been studied by Venne and Stanford (1979), Manney and Randel (1993), Bowman (1993), Pierce et al. (1994), Plumb et al. (1994), Manney et al. (1998), and Mizuta and Yoden (2002), among others. The synoptic sections of Figs. 8a,b show a breaking planetary wave in the polar night. This type of wave breaking on critical surfaces on the flanks of the polar night jet is similar to RWB poleward of the subtropical westerly jets, suggesting that this is most fundamentally westerly jet RWB.

A transition occurs across the stratopause region for RWB in the polar night. During the solstice seasons, gravity wave drag in the mesosphere accentuates the Lagrangian, thermally direct rising over the summer pole and sinking over the winter pole. This subsidence causes a warm anomaly to develop in the mesosphere in early winter and descend toward the stratopause (Hitchman et al. 1989). Garcia and Boville (1994) showed that the effects of mesospheric gravity wave drag are noticeable as low as ~30 km. There is considerable RWB within the descending anomaly near the stratopause, suggesting that descent of the separated

polar winter stratopause may be partly due to Rossby wave–mean flow interaction, via a mechanism similar to that proposed by Matsuno (1971). Indeed, Sassi et al. (2002) have shown that gravity wave drag induces a critical surface upon which upward-propagating planetary waves break: the mesospheric surf zone. Thus, although the RWB pattern is vertically continuous in the polar night, there is a transition from occasional poleward wave breaking on the stratospheric polar night jet to more vigorous wave breaking in the lower mesosphere.

3) SUMMER POLAR STRATOSPHERE

The vigorous RWB regime in the summer polar lower stratosphere decreases upward in strength, but not in frequency (Figs. 1, 2). At higher altitudes $\overline{P}_y$ can become negative, associated with a poleward decrease of $\overline{\theta}_z$ (Figs. 1a,b and 6b). In such weak PV gradients Rossby waves of a given amplitude can more easily lead to reversals. Hess and Holton (1985) argued that constituent variations near the summer pole are left over from the winter, being frozen debris with longer photochemical time scales than for PV. Miles and Grose (1986), however, observed extensive, coherent synoptic Rossby wave activity in the southern summer well into the stratosphere. Hitchman et al. (1999) documented several case studies of slowly propagating synoptic Rossby waves in the summer stratosphere over Alaska.

From consideration of the Charney–Drazin criterion and the location of the $\overline{u} = -5 \text{ m s}^{-1}$ surface, one would expect that synoptic Rossby wave activity would ascend well into the stratosphere during summer. In addition, the regions of $\overline{P}_y < 0$ in Figs. 1 and 6 suggest that mild baroclinic energy conversion could be occurring in the summer stratosphere. Mild EP flux divergence is seen in the summer upper stratosphere (Fig. 7). Piani and Norton (2002) diagnosed a similar feature in ECMWF data and discussed the possibility that instability can help mix the upper stratosphere, keeping it close to solid-body rotation. Note, however, that S decreases upward from the summer polar tropopause, consistent with evanescence from a tropospheric wave source.

Recent work on the evolution of the summer stratosphere by Lahoz et al. (2006, manuscript submitted to *Quart. J. Roy. Meteor. Soc.*) shows that constituents vary in concert with PV in the lower stratosphere, but variability in both decay into the upper stratosphere. Fahey and Ravishankara (1999) showed that some of the ozone decline is due to greater destruction by NO_x in strong sunlight. Hitchman et al. (1999) suggested that upwardly evanescent synoptic waves can contribute toward the observed decline in column ozone from ~450 to 250 Dobson units (DU, where 1 DU = 2.69×10^{16}

molecules cm^{-1}) during April to September over Alaska. These waves exist in the high-latitude lower stratosphere during all seasons, transporting ozone poleward and downward into the troposphere. From October through April in the NH this export is more than compensated by transport of ozone by planetary waves into the polar lower stratosphere, building to a maximum of ~450 DU. But from May through September, synoptic wave export continues after the planetary wave transport ceases, and column ozone amounts decline to ~250 DU. Absorption of upwardly evanescent synoptic waves in the summer stratosphere contributes to the poleward/downward Brewer–Dobson circulation, which advects low ozone air from the subtropical lower stratosphere.

b. Monsoon RWB in the tropical upper troposphere

Figures 3a–d show chronic, weak RWB in the tropical upper troposphere. Much of this RWB lies equatorward of monsoon anticyclones (Figs. 3a–d). The EP flux divergence from the tops of the monsoon anticyclones accounts for most of the tropical component of the alternating pattern along the tropopause (Fig. 7). Monsoon RWB occurs in association with quasi-steady Rossby wave packets in the Tropics forced by convection.

Monsoon anticyclones occur over Mexico and Tibet during JJA and over Amazonia, Africa, and near Indonesia during DJF. The Tropics and these anticyclones are characterized by small PV, created in convective updrafts where $\theta_z \leq 0$. These structures are quasi-steady Rossby wave solutions to tropical tropospheric heat sources (Sardeshmukh and Hoskins 1987; Gill 1980). From the definition of Rossby wave activity, anticyclonic stirring of air parcels is represented by $\overline{\delta y^2}$, with the Rossby source being aggregate convection. Convection creates a pair of anticyclones, with off-equatorial heating favoring a stronger one in the same hemisphere, such as the Tibetan high during boreal summer. The possibility for $P_y < 0$ is enabled by the convection, which creates the tropopausal anticyclonic pools of low static stability air (hence small PV), so that extratropical PV streamers wound around their equatorward sides easily cause reversals.

c. Inertial/barotropic RWB in the tropical middle atmosphere

A strikingly persistent and strong PV gradient is seen at the equator in the stratosphere in all seasons in both the NCEP and UKMO data (Figs. 1–4). It is flanked by surf zones with weak PV gradients and a compact relationship between v and P_y normalized by $(\bar{\theta}_z/\rho)\beta$, and

is typified by chronic, weak breaking. This structure may be due to a combined inertial-barotropic instability. The wintertime flow from the summer to winter hemisphere advects easterly angular momentum across the equator, rendering the winter subtropics inertially unstable (Dunkerton 1981). Inertial instability in the subtropical winter mesosphere should homogenize angular momentum from the equator to the latitude where $f = \bar{u}_y$, creating negatively curved flow over the equator, with an easterly jet on the summer side (Holton 1983; Hitchman 1985).

Barotropic instability of the subtropical easterly jet and its relationship to the 2-day, wavenumber-3 Rossby wave has been studied by Salby (1981), Plumb (1983), Burks and Leovy (1986), Limpasuvan and Leovy (1995), and Orsolini et al. (1997). Shuckburgh et al. (2001) showed that barotropic instability and associated mixing in the subtropics is enhanced on the flanks of QBO westerlies. These studies support the idea that traveling Rossby waves can amplify where $\overline{P}_y$ switches sign across the subtropics. Figure 6a shows that curvature of the subtropical easterly jet may be sufficient for $\overline{P}_y < 0$ on many days. Local RWB ensues, helping to trim wave amplitudes, keeping S small. The unique combination of inertial/barotropic instability underlying this RWB regime suggests a separate dynamical category. Since the Brewer–Dobson circulation flows through this region from summer to winter, one may conclude that inertial instability and RWB facilitate the meridional transport.

6. Conclusions

RWB statistics and PV gradient were calculated for each season from 320 to 2000 K in two long-term global datasets. Plan views and zonal mean sections provide an overview of the spatial distribution of seven breaking regimes, their seasonal dependence, and their relationships to quasi-stationary anticyclones, jet structures, the poles, and the equatorial stratosphere. Components of PV gradient and EP fluxes were examined and statistical relationships among v, S, and P_y were explored. RWB regimes coincide with EP flux divergence and convergence regions, consistent with violations of the nontransport theorem (Andrews et al. 1987).

Three different dynamical RWB types were suggested as a tentative metacategorization. Westerly Jet RWB occurs in association with Rossby waves growing and breaking poleward and equatorward on westerly jets. Within the winter polar vortex, vigorous RWB occurs in a region of near solid-body rotation, including the separated polar winter stratopause. RWB decays

upward in the summer polar stratosphere where β is small and $\overline{P}_y$ is often negative. This occurs in the anticyclonic relative vorticity of the weak summer easterly flow where $f\overline{\theta}_{yz} < 0$. Monsoon RWB occurs equatorward of tropopausal monsoon anticyclones in association with diverging Rossby wave activity. Inertial/barotropic RWB occurs near the subtropical easterly jets above the tropopause. The inertial instability of cross-equatorial flow in meridional shear leads to transport that sharpens the negative curvature of the easterly jets to the point of barotropic instability. The chronically enhanced narrow $\overline{P}_y$ maximum over the equator above the tropopause may be viewed as a result of a combined inertial-barotropic instability, all components of the cross-equatorial Lagrangian flow.

The complex relationship between PV gradient and RWB was explored statistically. Large PV gradients are consistent with low RWB, but large enough waves can overcome a given PV gradient. Breaking strength is linearly related to daily variability but not to PV gradient. Westerly jets appear to be minima in stirring, but mesoscale mixing and eddy shedding provide the requisite transport across the jets for the Lagrangian meridional circulation. The narrow regions of enhanced gradients in PV and constituents on the edges of the stratospheric surf zone are produced by quasi-horizontal flows associated with breaking waves of a much larger scale. Since these airmass boundaries are produced by differential advection associated with RWB, it is suggested that they be referred to as subtropical and subpolar stratospheric fronts (Palmen and Newton 1969).

REFERENCES

Andrews, D. G., J. R. Holton, and C. B. Leovy, 1987: *Middle Atmosphere Dynamics.* Academic Press, 489 pp.

Baldwin, M. P., and J. R. Holton, 1988: Climatology of the stratospheric polar vortex and planetary wave breaking. *J. Atmos. Sci.,* **45,** 1123–1142.

Berrisford, P., B. J. Hoskins, and E. Tyrlis, 2007: Blocking and Rossby wave breaking on the dynamical tropopause in the Southern Hemisphere. *J. Atmos. Sci.,* in press.

Birner, T., 2006: The fine-scale structure of the extratropical tropopause region. *J. Geophys. Res.,* **111,** D04104, doi:10.1029/2005JD006301.

Bower, A. S., 1991: A simple kinematic mechanism for mixing parcels across a meandering jet. *J. Phys. Oceanogr.,* **21,** 173–180.

Bowman, K. P., 1993: Large-scale isentropic mixing properties of the Antarctic polar vortex from analyzed winds. *J. Geophys. Res.,* **98,** 23 013–23 027.

Bretherton, F. B., 1966: Critical layer instability in baroclinic flows. *Quart. J. Roy. Meteor. Soc.,* **92,** 325–334.

Büker, M. L., M. H. Hitchman, G. J. Tripoli, R. B. Pierce, E. V. Browell, and M. A. Avery, 2005: Resolution dependence of cross-tropopause ozone transport over east Asia. *J. Geophys. Res.,* **110,** D03107, doi:10.1029/2004JD004739.

Burks, D., and C. B. Leovy, 1986: Planetary waves near the mesospheric easterly jet. *Geophys. Res. Lett.,* **13,** 193–196.

Butchart, N., and E. E. Remsberg, 1986: The area of the stratospheric polar vortex as a diagnostic for tracer transport on an isentropic surface. *J. Atmos. Sci.,* **43,** 1319–1339.

Danielsen, E. F., R. S. Hipskind, W. L. Starr, J. F. Vedder, S. E. Gaines, D. Kley, and K. K. Kelly, 1991: Irreversible transport in the stratosphere by internal waves of short vertical wavelength. *J. Geophys. Res.,* **96,** 17 433–17 452.

Doglioli, A. M., M. Veneziani, B. Blanke, S. Speich, and A. Griffa, 2006: A Lagrangian analysis of the Indian–Atlantic interocean exchange in a regional model. *Geophys. Res. Lett.,* **33,** L14611, doi:10.1029/2006GL026498.

Duan, J., and S. Wiggins, 1996: Fluid exchange across a meandering jet with quasiperiodic variability. *J. Phys. Oceanogr.,* **26,** 1176–1188.

Dunkerton, T. J., 1981: On the inertial instability of the equatorial middle atmosphere. *J. Atmos. Sci.,* **38,** 2354–2364.

Esler, J. G., and P. H. Haynes, 1999: Baroclinic wave breaking and the internal variability of the tropospheric circulation. *J. Atmos. Sci.,* **56,** 4014–4031.

Fahey, D. W., and A. R. Ravishankara, 1999: Summer in the stratosphere. *Science,* **285,** 208–210.

Fjortoft, R., 1950: Application of integral theorems in deriving criteria of stability for laminar flows and for the baroclinic circular vortex. *Geofys. Publ.,* **17,** 1–52.

Garcia, R. R., and B. A. Boville, 1994: "Downward control" of the mean meridional circulation and temperature distribution of the polar winter stratosphere. *J. Atmos. Sci.,* **51,** 2238–2245.

Gill, A. E., 1980: Some simple solutions for heat-induced tropical circulation. *Quart. J. Roy. Meteor. Soc.,* **106,** 447–462.

Hartmann, D. L., and P. Zuercher, 1998: Response of baroclinic life cycles to barotropic shear. *J. Atmos. Sci.,* **55,** 297–313.

Harvey, V. L., and M. H. Hitchman, 1996: A climatology of the Aleutian high. *J. Atmos. Sci.,* **53,** 2088–2101.

——, ——, R. B. Pierce, and T. D. Fairlie, 1999: Tropical high aerosol in the Aleutian anticyclone. *J. Geophys. Res.,* **104,** 6281–6290.

Haynes, P. H., 1985: Nonlinear instability of a Rossby-wave critical layer. *J. Fluid Mech.,* **161,** 493–511.

——, and E. Shuckburgh, 2000a: Effective diffusivity as a diagnostic of atmospheric transport, 1, Stratosphere. *J. Geophys. Res.,* **105,** 22 777–22 794.

——, and ——, 2000b: Effective diffusivity as a diagnostic of atmospheric transport, 2, Troposphere and lower stratosphere. *J. Geophys. Res.,* **105,** 22 795–22 810.

Hess, P. G., and J. R. Holton, 1985: The origin of temporal variance in long-lived trace constituents in the summer stratosphere. *J. Atmos. Sci.,* **42,** 1455–1463.

Hitchman, M. H., 1985: An observational study of wave-mean flow interaction in the equatorial middle atmosphere. Ph.D. dissertation, University of Washington, 365 pp.

——, C. B. Leovy, J. C. Gille, and P. L. Bailey, 1987: Quasi-stationary, zonally asymmetric circulations in the equatorial middle atmosphere. *J. Atmos. Sci.,* **44,** 2219–2236.

——, J. C. Gille, C. D. Rodgers, and G. Brasseur, 1989: The separated polar winter stratopause: A gravity wave driven climatological feature. *J. Atmos. Sci.,* **46,** 410–422.

——, M. McKay, and C. R. Trepte, 1994: A climatology of stratospheric aerosol. *J. Geophys. Res.,* **99,** 20 689–20 700.

——, M. L. Buker, and G. J. Tripoli, 1999: Influence of synoptic waves on column ozone during Arctic summer 1997. *J. Geophys. Res.,* **104,** 26 547–26 563.

——, ——, ——, R. B. Pierce, J. A. Al-Saadi, E. V. Browell, and M. A. Avery, 2004: A modeling study of an East Asian convective complex during March 2001. *J. Geophys. Res.,* **109,** D15S14, doi:10.1029/2003JD004312.

Holton, J. R., 1983: The influence of gravity wave breaking on the general circulation of the middle atmosphere. *J. Atmos. Sci.,* **40,** 2497–2507.

Hoskins, B. J., M. E. McIntyre, and A. W. Robertson, 1985: On the use and significance of isentropic potential vorticity maps. *Quart. J. Roy. Meteor. Soc.,* **111,** 877–946.

Kalnay, E., and Coauthors, 1996: The NCEP/NCAR 40-Year Reanalysis project. *Bull. Amer. Meteor. Soc.,* **77,** 437–471.

Kida, H., 1977: A numerical investigation of the atmospheric general circulation and stratosphere troposphere mass exchange: II. Lagrangian motion of the atmosphere. *J. Meteor. Soc. Japan,* **55,** 71–88.

Knox, J. A., and V. L. Harvey, 2005: Global climatology of inertial instability and Rossby wave breaking in the stratosphere. *J. Geophys. Res.,* **110,** D06108, doi:10.1029/2004JD005068.

Kritz, M. A., S. W. Rosner, E. F. Danielsen, and H. B. Selkirk, 1991: Air mass origins and troposphere-to-stratosphere exchange associated with midlatitude cyclogenesis and tropopause folding inferred from ^{7}Be measurements. *J. Geophys. Res.,* **96,** 17 405–17 414.

Lau, N.-C., 1978: On the three-dimensional structure of the observed transient eddy statistics of the Northern Hemisphere wintertime circulation. *J. Atmos. Sci.,* **35,** 1900–1923.

Limpasuvan, V., and C. B. Leovy, 1995: Observations of the 2-day wave near the southern summer stratopause. *Geophys. Res. Lett.,* **22,** 2385–2388.

Manney, G. L., and W. J. Randel, 1993: Instability at the winter stratopause: A mechanism for the 4-day wave. *J. Atmos. Sci.,* **50,** 3928–3938.

——, Y. J. Orsolini, H. C. Pumphrey, and A. E. Roche, 1998: The 4-day wave and transport of UARS tracers in the Austral polar vortex. *J. Atmos. Sci.,* **55,** 3456–3470.

Martius, O., C. Schwierz, and H. C. Davies, 2007: Breaking waves at the tropopause in the wintertime Northern Hemisphere: Climatological analyses of the orientation and the theoretical LC1/2 classification. *J. Atmos. Sci.,* **64,** in press.

Matsuno, T., 1971: A dynamical model of the sudden stratospheric warming. *J. Atmos. Sci.,* **28,** 1479–1494.

McIntyre, M. E., 1970: On the non-separable baroclinic parallel flow instability problem. *J. Fluid Mech.,* **40,** 273–306.

——, 1982: How well do we understand the dynamics of stratospheric warmings? *J. Meteor. Soc. Japan,* **60,** 37–65.

——, and T. N. Palmer, 1983: Breaking planetary waves in the stratosphere. *Nature,* **305,** 593–600.

——, and ——, 1984: The "surf zone" in the stratosphere. *J. Atmos. Terr. Phys.,* **46,** 825–839.

Methven, J., 2003: The influence of PV inversion on polar-vortex dynamics and passive-tracer simulations in atmosphere-like regimes. *Quart. J. Roy. Meteor. Soc.,* **129,** 1191–1215.

Miles, T., and W. L. Grose, 1986: Transient medium-scale wave activity in the summer stratosphere. *Bull. Amer. Meteor. Soc.,* **67,** 674–686.

Mizuta, R., and S. Yoden, 2002: Interannual variability of the 4-day wave and isentropic mixing in the polar vortex in midwinter of the Southern Hemisphere upper stratosphere. *J. Geophys. Res.,* **107,** 4798, doi:10.1029/2001JD002037.

Murphy, D. M., D. W. Fahey, M. H. Proffitt, S. C. Liu, K. R. Chan, C. S. Eubank, S. R. Kawa, and K. Kelly, 1993: Reactive nitrogen and its correlation with ozone in the lower stratosphere and upper troposphere. *J. Geophys. Res.,* **98,** 5325–5332.

Nakamura, H., M. Nakamura, and J. L. Anderson, 1997: The role of high- and low-frequency dynamics in blocking formation. *Mon. Wea. Rev.,* **125,** 2074–2093.

Nakamura, N., 1996: Two-dimensional mixing, edge formation, and permeability diagnosed in area coordinates. *J. Atmos. Sci.,* **53,** 1524–1537.

——, 2004: Quantifying asymmetric wavebreaking and two-way transport. *J. Atmos. Sci.,* **61,** 2735–2748.

Neu, J. L., L. C. Sparling, and R. A. Plumb, 2003: Variability of the subtropical "edges" in the stratosphere. *J. Geophys. Res.,* **108,** 4482, doi:10.1029/2002JD002706.

Newell, R. E., V. Thouret, J. Y. N. Cho, P. Stoller, A. Marenco, and H. G. Smit, 1999: Ubiquity of quasi-horizontal layers in the troposphere. *Nature,* **398,** 316–319.

Orsolini, Y. J., and W. B. Grant, 2000: Seasonal formation of nitrous oxide laminae in the mid and low latitude stratosphere. *Geophys. Res. Lett.,* **27,** 1119–1122.

——, V. Limpasuvan, and C. B. Leovy, 1997: The tropical stratopause in the UKMO stratospheric analysis: Evidence for a 2-day wave and inertial circulations. *Quart. J. Roy. Meteor. Soc.,* **123,** 1707–1724.

O'Sullivan, D. J., and M. H. Hitchman, 1992: Inertial instability and Rossby wave breaking in a numerical model. *J. Atmos. Sci.,* **49,** 991–1002.

Palmen, E., and C. W. Newton, 1969: *Atmospheric Circulation Systems.* Academic Press, 603 pp.

Peixoto, J. P., and A. H. Oort, 1992: *Physics of Climate.* American Institute of Physics, 520 pp.

Peters, D., and D. W. Waugh, 1996: Influence of barotropic shear on the poleward advection of upper-tropospheric air. *J. Atmos. Sci.,* **53,** 3013–3031.

——, and ——, 2003: Rossby wave breaking in the Southern Hemisphere wintertime upper troposphere. *Mon. Wea. Rev.,* **131,** 2623–2634.

Piani, C., and W. A. Norton, 2002: Solid-body rotation in the northern hemisphere summer stratosphere. *Geophys. Res. Lett.,* **29,** 2117, doi:10.1029/2002GL016079.

Pierce, R. B., T. D. Fairlie, W. L. Grose, R. Swinbank, and A. O'Neill, 1994: Mixing processes within the polar night jet. *J. Atmos. Sci.,* **51,** 2957–2972.

Pierrehumbert, R. T., 1991: Large-scale horizontal mixing in planetary atmospheres. *Phys. Fluids,* **3A,** 1250–1260.

Plumb, R. A., 1983: Baroclinic instability of the summer mesosphere: A mechanism for the quasi-two-day wave? *J. Atmos. Sci.,* **40,** 262–270.

——, and Coauthors, 1994: Intrusions into the lower stratospheric

Arctic vortex during the winter of 1991–1992. *J. Geophys. Res.,* **99,** 1089–1105.

Postel, G. A., 1994: Zonally asymmetric large-scale dynamics in the upper troposphere and lower stratosphere. M.S. thesis, Department of Atmospheric and Oceanic Sciences, University of Wisconsin—Madison, 77 pp.

——, and M. H. Hitchman, 1999: Climatology of Rossby wave breaking along the subtropical tropopause. *J. Atmos. Sci.,* **56,** 359–373.

——, and ——, 2001: Observational diagnosis of a Rossby wave breaking event along the subtropical tropopause. *Mon. Wea. Rev.,* **129,** 2555–2569.

Ray, E. A., K. H. Rosenlof, E. Richard, D. Parish, and R. Jakoubek, 2005: Distributions of ozone in the region of the subtropical jet: An analysis of *in situ* aircraft measurements. *J. Geophys. Res.,* **109,** D08106, doi:10.1029/2003JD004143.

Rhines, P. B., and W. R. Young, 1982: Potential vorticity homogenization in planetary gyres. *J. Fluid Mech.,* **122,** 347–367.

Richardson, L. F., 1922: *Weather Prediction by Numerical Process.* Cambridge University Press, 236 pp.

Rossby, C.-G., 1947: On the distribution of angular velocity in gaseous envelopes under the influence of large-scale horizontal mixing processes. *Bull. Amer. Meteor. Soc.,* **28,** 53–68.

Salby, M. L., 1981: Rossby normal modes in nonuniform background configurations. Part II: Equinox and solstice conditions. *J. Atmos. Sci.,* **38,** 1827–1840.

Sardeshmukh, P. D., and B. J. Hoskins, 1987: The generation of global rotational flow by steady idealized tropical divergence. *J. Atmos. Sci.,* **45,** 1228–1251.

Sassi, F., R. R. Garcia, B. A. Boville, and H. Liu, 2002: On temperature inversions and the mesospheric surf zone. *J. Geophys. Res.,* **107,** 4380, doi:10.1029/2001JD001525.

Sato, K., and T. J. Dunkerton, 2002: Layered structure associated with low potential vorticity near the tropopause seen in high-resolution radiosondes over Japan. *J. Atmos. Sci.,* **59,** 2782–2800.

Scott, R. K., and J.-P. Cammas, 2002: Wave breaking and mixing at the subtropical tropopause. *J. Atmos. Sci.,* **59,** 2347–2361.

Shine, K., 1987: The middle atmosphere in the absence of dynamical heat fluxes. *Quart. J. Roy. Meteor. Soc.,* **113,** 603–633.

Shuckburgh, E., W. Norton, A. Iwi, and P. Haynes, 2001: Influence of the quasi-biennial oscillation on isentropic transport and mixing in the tropics and subtropics. *J. Geophys. Res.,* **106,** 14 327–14 337.

Simmons, A. J., and B. J. Hoskins, 1978: The life cycles of some nonlinear baroclinic waves. *J. Atmos. Sci.,* **35,** 414–432.

Sprenger, M., and H. Wernli, 2003: A Northern Hemisphere climatology of cross-tropopause exchange for the ERA15 time period (1979–1993). *J. Geophys. Res.,* **108,** 8521, doi:10.1029/2002JD002636.

Swinbank, R., and A. O'Neill, 1994: The UKMO dataset. *Mon. Wea. Rev.,* **122,** 686–702.

Thorncroft, C. D., B. J. Hoskins, and M. E. McIntyre, 1993: Two paradigms of baroclinic wave life cycle behavior. *Quart. J. Roy. Meteor. Soc.,* **119,** 17–55.

Tuck, A. F., and Coauthors, 1992: Polar stratospheric cloud processed air and potential vorticity in the Northern Hemisphere lower stratosphere at midlatitudes during winter. *J. Geophys. Res.,* **97,** 7883–7904.

Venne, D. E., and J. L. Stanford, 1979: Observation of a 4-day temperature wave in the polar winter stratosphere. *J. Atmos. Sci.,* **36,** 2016–2019.

Wallace, J. M., 1978: Trajectory slopes, countergradient heat fluxes and mixing by lower stratospheric waves. *J. Atmos. Sci.,* **35,** 554–558.

Waugh, D. W., and L. M. Polvani, 2000: Climatology of intrusions into the tropical upper troposphere. *Geophys. Res. Lett.,* **27,** 3857–3860.

Wiggins, S., and J. M. Ottino, 2004: Foundations of chaotic mixing. *Philos. Trans. Roy. Soc. London,* **362A,** 937–970.

Wilson, J. C., W. T. Lai, and S. D. Smith, 1991: Measurements of condensation nuclei above the jet stream: Evidence for cross-jet transport by waves and new particle formation at high latitudes. *J. Geophys. Res.,* **96,** 17 415–17 423.